

Neutron Capture Cross Section of Unstable ^{63}Ni : Implications for Stellar Nucleosynthesis

C. Lederer,^{1,2} C. Massimi,³ S. Altstadt,² J. Andrzejewski,⁴ L. Audouin,⁵ M. Barbagallo,⁶ V. Bécáres,⁷ F. Bečvář,⁸ F. Belloni,⁹ E. Berthoumieux,^{9,10} J. Billowes,¹¹ V. Boccone,¹⁰ D. Bosnar,¹² M. Brugger,¹⁰ M. Calviani,¹⁰ F. Calviño,¹³ D. Cano-Ott,⁷ C. Carrapiço,¹⁴ F. Cerutti,¹⁰ E. Chiaveri,^{9,10} M. Chin,¹⁰ N. Colonna,⁶ G. Cortés,¹³ M. A. Cortés-Giraldo,¹⁵ M. Diakaki,¹⁶ C. Domingo-Pardo,¹⁷ I. Duran,¹⁸ R. Dressler,¹⁹ N. Dzysiuk,²⁰ C. Eleftheriadis,²¹ A. Ferrari,¹⁰ K. Fraval,⁹ S. Ganesan,²² A. R. García,⁷ G. Giubrone,¹⁷ M. B. Gómez-Hornillos,¹³ I. F. Gonçalves,¹⁴ E. González-Romero,⁷ E. Griesmayer,²³ C. Guerrero,¹⁰ F. Gunsing,⁹ P. Gurusamy,²² D. G. Jenkins,²⁴ E. Jericha,²³ Y. Kadi,¹⁰ F. Käppeler,²⁵ D. Karadimos,¹⁶ N. Kivel,¹⁹ P. Koehler,²⁶ M. Kokkoris,¹⁶ G. Korschinek,²⁷ M. Krčička,⁸ J. Kroll,⁸ C. Langer,² H. Leeb,²³ L. S. Leong,⁵ R. Losito,¹⁰ A. Manousos,²¹ J. Marganec,⁴ T. Martínez,⁷ P. F. Mastinu,²⁰ M. Mastromarco,⁶ M. Meaze,⁶ E. Mendoza,⁷ A. Mengoni,²⁸ P. M. Milazzo,²⁹ F. Mingrone,³ M. Mirea,³⁰ W. Mondelaers,³¹ C. Paradela,¹⁸ A. Pavlik,¹ J. Perkowski,⁴ M. Pignatari,³² A. Plompen,³¹ J. Praena,¹⁵ J. M. Quesada,¹⁵ T. Rauscher,^{32,33} R. Reifarth,² A. Riego,¹³ F. Roman,^{10,30} C. Rubbia,^{10,34} R. Sarmiento,¹⁴ P. Schillebeeckx,³¹ S. Schmidt,² D. Schumann,¹⁹ G. Tagliente,⁶ J. L. Tain,¹⁷ D. Tarrío,¹⁸ L. Tassan-Got,⁵ A. Tsinganis,^{10,16} S. Valenta,⁸ G. Vannini,³ V. Variale,⁶ P. Vaz,¹⁴ A. Ventura,²⁸ R. Versaci,¹⁰ M. J. Vermeulen,²⁴ V. Vlachoudis,¹⁰ R. Vlastou,¹⁶ A. Wallner,^{1,35} T. Ware,¹¹ M. Weigand,² C. Weiß,²³ T. J. Wright,¹¹ and P. Žugec¹²

(n_TOF Collaboration)

¹University of Vienna, Faculty of Physics, 1090 Vienna, Austria

²Johann-Wolfgang-Goethe Universität, 60438 Frankfurt, Germany

³Dipartimento di Fisica, Università di Bologna, and Sezione INFN di Bologna, 40100 Bologna, Italy

⁴Uniwersytet Łódzki, 90131 Lodz, Poland

⁵Centre National de la Recherche Scientifique/IN2P3-IPN, 91406 Orsay, France

⁶Istituto Nazionale di Fisica Nucleare, 70125 Bari, Italy

⁷Centro de Investigaciones Energeticas Medioambientales y Tecnológicas (CIEMAT), 28040 Madrid, Spain

⁸Charles University, CZ-180 00 Prague, Czech Republic

⁹Commissariat à l'Énergie Atomique (CEA) Saclay-Irfu, 91191 Gif-sur-Yvette, France

¹⁰European Organization for Nuclear Research (CERN), CH-1211 Geneva, Switzerland

¹¹University of Manchester, Oxford Road, Manchester M13 9PL, United Kingdom

¹²Department of Physics, Faculty of Science, University of Zagreb, 10002 Zagreb, Croatia

¹³Universitat Politècnica de Catalunya, 08028 Barcelona, Spain

¹⁴IST/ITN, Instituto Superior Técnico, Universidade Técnica Lisboa, Estrada Nacional 10, 2695-066 Bobadela, Portugal

¹⁵Universidad de Sevilla, 41080 Sevilla, Spain

¹⁶National Technical University of Athens (NTUA), 15780 Athens, Greece

¹⁷Instituto de Física Corpuscular, CSIC-Universidad de Valencia, 46071 Valencia, Spain

¹⁸Universidade de Santiago de Compostela, 15782 Santiago de Compostela, Spain

¹⁹Paul Scherrer Institut, 5232 Villigen PSI, Switzerland

²⁰Istituto Nazionale di Fisica Nucleare, Laboratori Nazionali di Legnaro, 35020 Legnaro, Italy

²¹Aristotle University of Thessaloniki, 54124 Thessaloniki, Greece

²²Bhabha Atomic Research Centre (BARC), Trombay, 400085 Mumbai, India

²³Atominstytut, Technische Universität Wien, 1040 Vienna, Austria

²⁴University of York, Heslington, York YO10 5DD, United Kingdom

²⁵Karlsruhe Institute of Technology, Campus Nord, Institut für Kernphysik, 76021 Karlsruhe, Germany

²⁶Oak Ridge National Laboratory (ORNL), Oak Ridge, Tennessee 37831, USA

²⁷Technical University of Munich, 80333 Munich, Germany

²⁸Agenzia nazionale per le nuove tecnologie, l'energia e lo sviluppo economico sostenibile (ENEA), 40129 Bologna, Italy

²⁹Istituto Nazionale di Fisica Nucleare, 34127 Trieste, Italy

³⁰Horia Hulubei National Institute of Physics and Nuclear Engineering, P.O. Box MG-6, 077125 Bucharest Magurele, Romania

³¹European Commission JRC, Institute for Reference Materials and Measurements, Retieseweg 111, B-2440 Geel, Belgium

³²Department of Physics-University of Basel, 4056 Basel, Switzerland

³³Institute of Nuclear Research (ATOMKI), H-4001 Debrecen, POB 51, Hungary

³⁴Laboratori Nazionali del Gran Sasso dell'INFN, 67010 Assergi (AQ), Italy

³⁵Research School of Physics and Engineering, Australian National University, ACT 0200, Australia

(Received 8 October 2012; published 8 January 2013)

The $^{63}\text{Ni}(n, \gamma)$ cross section has been measured for the first time at the neutron time-of-flight facility n_TOF at CERN from thermal neutron energies up to 200 keV. In total, capture kernels of 12 (new)

resonances were determined. Maxwellian averaged cross sections were calculated for thermal energies from $kT = 5\text{--}100$ keV with uncertainties around 20%. Stellar model calculations for a $25M_{\odot}$ star show that the new data have a significant effect on the s -process production of ^{63}Cu , ^{64}Ni , and ^{64}Zn in massive stars, allowing stronger constraints on the Cu yields from explosive nucleosynthesis in the subsequent supernova.

DOI: 10.1103/PhysRevLett.110.022501

PACS numbers: 25.40.Lw, 25.40.Ny, 26.20.Kn, 27.50.+e

The weak component of the astrophysical s process observed in the solar system abundance distribution includes the s -process species between Fe and Sr ($60 < A < 90$) [1]. Most of them are generated in massive stars during convective He core burning and convective C shell burning via the activation of the neutron source reaction $^{22}\text{Ne}(\alpha, n)^{25}\text{Mg}$ [2–6]. The long-lived radioisotope ^{63}Ni ($t_{1/2} = 101.2 \pm 1.5$ yr [7]) is located along the neutron capture path, and in typical weak s -process conditions it may become a branching point, when the neutron capture time scale is comparable with its stellar β -decay rate.

In particular, at the end of He core burning the neutron source $^{22}\text{Ne}(\alpha, n)^{25}\text{Mg}$ is activated at temperatures around 0.3 GK (GK = 10^9 K), corresponding to a Maxwellian neutron energy distribution for a thermal energy of $kT = 26$ keV. At this stage, neutron densities are too weak for a subsequent neutron capture on ^{63}Ni (with central peak neutron density on the order of 10^7 cm $^{-3}$, e.g., Refs. [5,6]) and more than 90% of the ^{63}Ni produced decays to ^{63}Cu . However, the s -process material is partly reprocessed during C shell burning, where the $^{22}\text{Ne}(\alpha, n)^{25}\text{Mg}$ neutron source is reactivated at much higher temperatures of about 1 GK, corresponding to a thermal energy of $kT = 90$ keV.

During this second stage, neutron densities are orders of magnitude higher, reaching a maximum of $10^{11\text{--}12}$ cm $^{-3}$ [8]. At the ^{63}Ni branching point, the high neutron densities favor neutron capture producing ^{64}Ni , bypassing the production of ^{63}Cu despite the strong temperature dependence of the ^{63}Ni β -decay rate (at C shell burning temperatures the half-life of ^{63}Ni decreases to a few years [9]). In these conditions, the amount of ^{63}Cu generated during He core burning is partially depleted in the C shell, but the final ^{63}Cu abundance will increase thanks to the later radiogenic decay of the ^{63}Ni accumulated in the C shell burning phase [8]. In Fig. 1, we show the neutron capture path in the

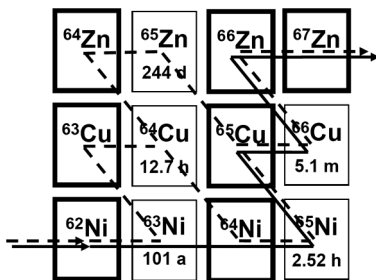


FIG. 1. The s -process reaction path in the Ni-Cu-Zn region during He core burning (dashed lines) and C shell burning (solid lines).

Ni-Cu-Zn region during He core and at high neutron density during C shell burning. Up to now the stellar cross section of $^{63}\text{Ni}(n, \gamma)^{64}\text{Ni}$ relied on calculations or extrapolations of experimental values at thermal neutron energies (0.025 eV) [10–12]. Theoretical predictions for the Maxwellian averaged cross section (MACS) at $kT = 30$ keV are ranging from 24 to 54 mb [13–17]. The currently recommended value quoted by the compilation KADoNiS [17] is 31 ± 6 mb. Because such calculations are vulnerable to large systematic uncertainties, measurements have been attempted at Los Alamos National Laboratory [18] and at CERN. In this Letter we report on the first experimental results for the ^{63}Ni cross section at stellar energies obtained at the n_TOF facility at CERN.

The measurement was performed at the neutron time-of-flight facility n_TOF located at CERN. Neutrons are produced via spallation reactions of 20 GeV/c protons from the Proton Synchrotron with a massive Pb target. With the high intensity of the pulsed proton beam, the repetition rate of 0.4 Hz, a short proton pulse width of 6 ns, and a neutron flight path of 185 m, the n_TOF facility is unique for the combination of a high neutron energy resolution and a high instantaneous neutron flux. A more detailed description of the facility can be found in Ref. [19] and references therein.

The ^{63}Ni sample was produced by irradiating highly enriched ^{62}Ni in a thermal reactor [12,20,21]. Since the irradiation took place more than 20 years ago, the original ^{63}Ni fraction had partially decayed to ^{63}Cu . To avoid background due to $^{63}\text{Cu}(n, \gamma)^{64}\text{Cu}$ reactions, this ^{63}Cu impurity has been chemically separated prior to the (n, γ) measurement. The originally metallic target was dissolved in concentrated nitric acid and the copper fraction was precipitated as CuS using gaseous H_2S . The remaining solution was treated with NaOH to precipitate $\text{Ni}(\text{OH})_2$, which was calcinated at 800°C to form NiO. By means of mass spectrometry, the $^{63}\text{Ni}/^{62}\text{Ni}$ ratio in the sample was determined to 0.123 ± 0.001 , and the contribution from other Ni isotopes was found to be $\leq 1\%$. In total, 1156 mg NiO powder were encapsulated in a thin-walled cylinder made of PEEK (polyether ether ketone, net mass 180 mg) to produce a sample 20 mm in diameter and 2.2 mm in thickness.

The neutron capture yield was measured as a function of neutron energy by detecting the prompt capture γ rays with a pair of liquid C_6D_6 scintillation detectors. These detectors are optimized to exhibit a very low sensitivity to neutrons, thus minimizing the background produced by neutrons scattered on the sample [22]. The dependence of the detection efficiency on γ -ray energy and the effect of the γ -ray

threshold of 250 keV were corrected using the pulse height weighting technique [23,24]. By application of a pulse-height dependent weight on the deposited γ energy, the detection efficiency becomes a linear function of the excitation energy of the compound nucleus, $\varepsilon \approx k \times E_c$. Choosing $k = 1 \text{ MeV}^{-1}$, the capture yield can be obtained as

$$Y = N \frac{C_w}{\Phi E_c}, \quad (1)$$

where C_w are the weighted, background-subtracted counts, Φ denotes the relative neutron flux, and N is a normalization factor for the absolute capture yield. The normalization factor was determined via the saturated resonance technique [25] in an additional run with a Au sample of the same size as the Ni sample. The Au sample was chosen such that the gold resonance at 4.9 eV is saturated, which means that all neutrons of that energy are absorbed in the sample, thus providing a measure for the absolute neutron flux at 4.9 eV. The energy dependence of the neutron flux was measured relative to the standard cross sections $^{10}\text{B}(n, \alpha)$ and $^6\text{Li}(n, \alpha)$ up to 150 keV and $^{235}\text{U}(n, f)$ at higher energies. Because the size of the neutron beam changes slightly with neutron energy, the normalization factor N , related to the fraction of the neutron beam intercepted by the sample, changes as well. This effect was taken into account by simulations of the neutron beam profile [19].

The experimental background was determined in dedicated runs with an empty PEEK container, with a ^{62}Ni sample of the same diameter, and in runs without neutron beam. Additionally, the neutron capture yield has been measured with a set of neutron filters located about 50 m upstream of the sample. These W, Mo, and Al filters are thick enough to exhibit black resonances at certain energies, so that all neutrons in these windows are completely removed from the beam and do not reach the sample. Accordingly, the level in the corresponding dips in these spectra is expected to represent the experimental background. When the run with filters was repeated using only the empty container, the same background level was observed in the filter dips, thus confirming the background measured with the empty sample container. Figure 2 shows a comparison of the capture yield of the ^{63}Ni sample, the empty PEEK container, and the ^{62}Ni sample. The background from the radioactivity of the ^{63}Ni sample and from ambient radiation, which was obtained from a measurement without neutron beam, is given as well. Between 100 eV and 2 keV four resonances are visible in the spectrum of the ^{63}Ni sample, which are obviously not correlated with the ^{62}Ni content. The first of these resonances (marked by an arrow) can be attributed to a resonance in the $^{59}\text{Ni}(n, \gamma)$ reaction [26], expected at that neutron energy and compatible with the measured 0.03% impurity of ^{59}Ni in our sample. The other three resonances are clearly attributable to the $^{63}\text{Ni}(n, \gamma)$ channel. This holds also for several other resonances up to neutron energies of 55 keV, for which the capture kernels

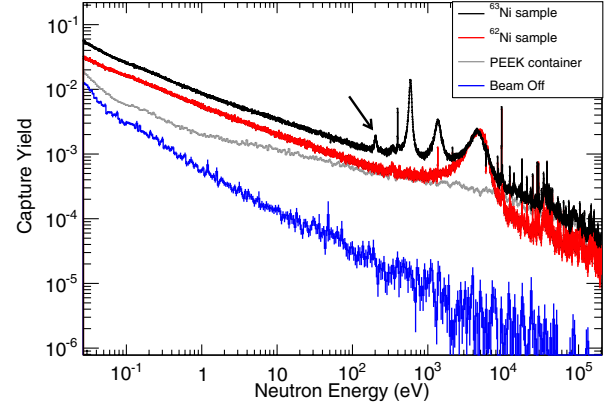


FIG. 2 (color online). Capture yield of the ^{63}Ni sample (black) compared to the empty PEEK container and to the spectrum obtained with a pure ^{62}Ni sample. The background from the activity of the sample and from ambient radiation is almost negligible at keV energies. The capture yield of the ^{62}Ni sample was scaled for the ^{62}Ni mass present in the ^{63}Ni sample. The first resonance at 203 eV (marked by an arrow) is assigned to a small impurity of ^{59}Ni in the sample.

$$A_\gamma = \frac{1}{2\pi^2 \lambda^2} \int_{-\infty}^{+\infty} \sigma(E) dE = g_s \frac{\Gamma_n \Gamma_\gamma}{\Gamma_n + \Gamma_\gamma}, \quad (2)$$

characterizing the strength of the resonance, could be deduced by a resonance shape analysis with the R -matrix code SAMMY [27] (Table I). The capture kernel is determined by the spin statistical factor g_s , the neutron width Γ_n , and the radiative width Γ_γ . For two resonances the orbital angular momentum ℓ , derived from the shape of the resonance, is also given. The neutron energy interval between 2 and 8 keV is dominated by the strong resonance in $^{62}\text{Ni}(n, \gamma)$ at 4.6 keV; therefore, smaller resonances in $^{63}\text{Ni}(n, \gamma)$ might be invisible due to this background. In summary, 12 levels in ^{64}Ni were observed for the first time.

As a consequence of the small sample mass, the signal-to-background ratio starts to deteriorate already above 10 keV. Accordingly, it is increasingly difficult to identify resonances with confidence at higher energies. Thus, MACSS were calculated using resonance parameters only below 10 keV, whereas averaged cross section data have been determined from 10 keV to 200 keV. These data were

TABLE I. Resonance energies E_r (laboratory energy) and capture kernels A_γ for the $^{63}\text{Ni}(n, \gamma)$ reaction. For resonances marked with an asterisk the orbital angular momentum $\ell = 0$ could be deduced from the resonance shape.

E_r (eV)	A_γ (meV)	E_r (eV)	A_γ (meV)
397.96 ± 0.04	5.7 ± 0.4	9776 ± 3	100 ± 10
$587.25 \pm 0.09^*$	340 ± 20	13984 ± 3	131 ± 45
$1366 \pm 1^*$	810 ± 40	17127 ± 4	108 ± 59
8634 ± 2	45 ± 9	19561 ± 6	130 ± 20
8981 ± 3	50 ± 10	32330 ± 10	500 ± 200
9154 ± 4	43 ± 9	54750 ± 30	700 ± 200

TABLE II. Maxwellian averaged cross sections (in mb) of $^{63}\text{Ni}(n, \gamma)$ compared to previously recommended values based on theoretical predictions [17]. The respective contributions from resonances below 10 keV (RC) are listed separately. Uncertainties are 1σ .

kT (keV)	KADoNiS		This work	
		RC		Total
5	112	174 ± 6	$224 \pm 8_{\text{stat}} \pm 45_{\text{syst}}$	
10	66	51 ± 2	$129.5 \pm 7.1 \pm 25.9$	
15	50	24 ± 1	$101.3 \pm 6.9 \pm 20.3$	
20	41	14 ± 1	$85.5 \pm 6.4 \pm 17.1$	
25	35	9.3 ± 0.4	$74.9 \pm 5.9 \pm 15.0$	
30	31 ± 6	6.6 ± 0.3	$66.7 \pm 5.4 \pm 13.3$	
40	25	3.8 ± 0.2	$54.5 \pm 4.6 \pm 10.9$	
50	20	2.4 ± 0.1	$45.6 \pm 3.9 \pm 9.1$	
60	17	1.7 ± 0.1	$38.8 \pm 3.4 \pm 7.8$	
80	13	0.97 ± 0.05	$29.1 \pm 2.7 \pm 5.8$	
100	10	0.63 ± 0.03	$22.5 \pm 2.1 \pm 4.5$	

obtained by subtraction of the yield measured with the ^{62}Ni sample after it had been properly scaled for the ^{62}Ni content of the ^{63}Ni sample. The background due to oxygen is negligibly small because of its very small (n, γ) cross section.

The MACSs for thermal energies from $kT = 5\text{--}100$ keV are listed in Table II, together with the theoretical predictions in the KADoNiS compilation [17]. Our results are approximately a factor of 2 higher than the calculated cross section. The total systematic uncertainties in our results of 20% are mainly due to subtraction of the background and the effect of sample impurities—particularly in the region between 2 and 8 keV, where the spectrum is dominated by the 4.6 keV resonance in $^{62}\text{Ni}(n, \gamma)$. Comparably minor contributions to the systematic uncertainty are caused by the neutron flux (3%–5%), the pulse height weighting technique (2%), the flux normalization (1%), and the $^{63}\text{Ni}/^{62}\text{Ni}$ ratio (1.6%).

The impact of our new results was investigated for the s process in a full stellar model for a $25M_{\odot}$ star with an initial metal content $Z = 0.02$. The complete nucleosynthesis was followed with the postprocessing NuGrid code MPPNP [28]. The stellar rates were obtained by combining the measured $^{63\text{gs}}\text{Ni}(n, \gamma)^{64}\text{Ni}$ cross sections and theoretically predicted contributions to the stellar rate due to $^{63}\text{Ni}^*(n, \gamma)^{64}\text{Ni}$ reactions as described in Ref. [29]. While the contribution of $^{63\text{gs}}\text{Ni}(n, \gamma)^{64}\text{Ni}$ reactions to the stellar rate is still around 90% at He core burning temperatures, it drops to around 40% at the higher temperature in the C shell burning phase. Because of the larger uncertainties of the $^{63}\text{Ni}^*(n, \gamma)^{64}\text{Ni}$ cross sections, the uncertainty of the stellar rate increases with temperature. Apart from the reaction cross sections, the final abundance pattern is also affected by the temperature dependence of the radioactive decay rates under stellar conditions. In the investigated mass region the concerned rates for the β^-

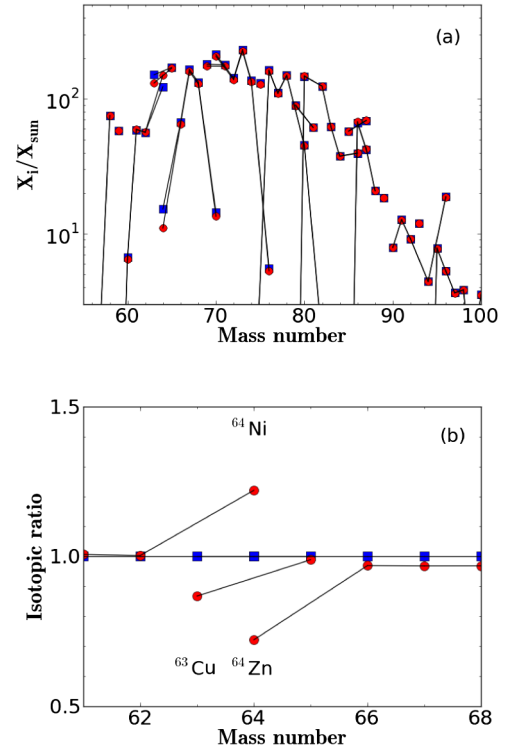


FIG. 3 (color online). (a) Final isotopic s -process distributions using the new measured ^{63}Ni MACS (red circles) and the MACS quoted by KADoNiS (blue squares) [17]. The distribution is normalized to solar system abundances. (b) Ratio of the two distributions in (a), zoomed in the Ni-Cu-Zn mass region. Isotopes of the same element are connected by solid lines.

decay of ^{63}Ni and the β^+/β^- decays of ^{64}Cu have been adopted from Ref. [9]. By variation within reasonable limits [8], it was found that the decay rates of both isotopes have a comparably small effect on the investigated abundances, because the reaction flow in the ^{63}Ni branching is governed by the neutron density conditions, which lead either to much lower or much higher (n, γ) rates during core He and C shell burning, respectively.

The calculated abundance distribution from Fe to Zr shown in Fig. 3 represents the s abundances after core He and C shell burning, i.e., prior to the supernova explosion, at a point where the nucleosynthesis yields are well characterized by the model [8]. The distribution is compared in Fig. 3 to the one obtained with the neutron capture rates of the KADoNiS evaluation [17]. The ratio of the two distributions in the lower panel of Fig. 3 shows that the new ^{63}Ni cross section affects only a few isotopes between Ni and Zn. An enhancement of about 20% is found for ^{64}Ni , while ^{63}Cu is depleted by about 15%. As the ^{65}Cu yields remain essentially unchanged, the isotopic ratio $^{63}\text{Cu}/^{65}\text{Cu}$ is correspondingly reduced at the end of C shell burning. ^{64}Zn is depleted as well (by about 30%), because ^{63}Cu and ^{64}Zn are populated by the nucleosynthesis channel following the β^- branch $^{62}\text{Ni}(n, \gamma)^{63}\text{Ni}(\beta^-)^{63}\text{Cu}(n, \gamma)^{64}\text{Cu}(\beta^-)^{64}\text{Zn}$. However, the s -process contribution to ^{64}Zn remains

marginal as this isotope results predominantly from later explosive nucleosynthesis during core collapse supernovae [30]. Also the propagation effect of the new MACS of ^{63}Ni on heavier s -process species is rather small, of the order of a few percent.

Although the s -process component at the end of convective C shell burning is well defined by these calculations, the abundances in the Ni-Cu-Zn region may be affected by following burning stages (for instance, the possible merging of shells [31]) and by the subsequent supernova explosion before enriching the interstellar medium. Given the complexity of this scenario, the final abundances are yet subject to considerable uncertainty as emphasized by several sensitivity studies [8,31,32]. Nevertheless, the present results represent a fundamental improvement in constraining the weak s -process component from the convective He core burning and convective C shell burning phases. A better knowledge of the preexplosive weak s -process component will allow to also better define the following explosive contribution to the copper inventory, once robust theoretical predictions are compared with spectroscopic observations. Another relevant observational constraint is given by the copper isotopic ratio in the Solar System, where the s process in massive stars provides the dominant contribution ([8], and references therein).

In summary, we measured the energy-dependent $^{63}\text{Ni}(n, \gamma)$ cross section at the n_TOF facility providing the first experimental results for MACSs at stellar neutron energies. The MACSs ranging from $kT = 5\text{--}100$ keV exhibit total uncertainties of 20%–22% and are about a factor of 2 higher than the theoretical prediction of the KADoNiS compilation. Our results improve one of the main nuclear uncertainties affecting theoretical predictions for the abundances of ^{63}Cu , ^{64}Ni , and ^{64}Zn in s -process rich ejecta of core collapse supernovae. Furthermore, these results are a fundamental step to constrain the contribution from explosive nucleosynthesis to these species.

The authors would like to thank H. Danninger and C. Gierl of the Technical University of Vienna for their help preparing the ^{62}Ni sample. This work was partly supported by the Austrian Science Fund (FWF), Projects No. P20434 and No. I428. M. P. also acknowledges the support from the Ambizione grant of the Swiss NSF, the NSF Grants No. PHY 02-16783 and No. PHY 09-22648 (Joint Institute for Nuclear Astrophysics, JINA), EU Grant No. MIRG-CT-2006-046520, and EuroGenesis. T. R. acknowledges support from EuroGenesis, the FP7 ENSAR/THEXO project, and a ‘‘Distinguished Guest Scientist Fellowship’’ from the Hungarian Academy of Sciences.

[1] F. Käppeler, H. Beer, and K. Wisshak, *Rep. Prog. Phys.* **52**, 945 (1989).

[2] J. G. Peters, *Astrophys. J.* **154**, 225 (1968).

- [3] R. G. Couch, A. B. Schmiedekamp, and W. D. Arnett, *Astrophys. J.* **190**, 95 (1974).
- [4] S. A. Lamb, W. M. Howard, J. W. Truran, and I. Iben, *Astrophys. J.* **217**, 213 (1977).
- [5] C. M. Raiteri, M. Busso, G. Picchio, and R. Gallino, *Astrophys. J.* **371**, 665 (1991).
- [6] C. M. Raiteri, M. Busso, G. Picchio, R. Gallino, and L. Pulone, *Astrophys. J.* **367**, 228 (1991).
- [7] R. Colle, B. E. Zimmermann, P. Cassette, and L. Laureano-Perez, *Appl. Radiat. Isot.* **66**, 60 (2008).
- [8] M. Pignatari, R. Gallino, M. Heil, M. Wiescher, F. Käppeler, F. Herwig, and S. Bisterzo, *Astrophys. J.* **710**, 1557 (2010).
- [9] K. Langanke and G. Martinez-Pinedo, *Nucl. Phys.* **A673**, 481 (2000).
- [10] I. L. Barnes, S. B. Garfinkel, and W. B. Mann, *Appl. Radiat. Isot.* **22**, 777 (1971).
- [11] H. Michael, A. Neubert, and H. Nickel, *Appl. Radiat. Isot.* **25**, 183 (1974).
- [12] A. Harder, S. Michaelsen, A. Jungclaus, K. P. Lieb, A. P. Williams, H. G. Börner, and M. Trautmannsheimer, *Z. Phys. A* **343**, 7 (1992).
- [13] S. Woosley, W. Fowler, J. Holmes, and B. Zimmermann, *At. Data Nucl. Data Tables* **22**, 371 (1978).
- [14] M. Harris, *Astrophys. Space Sci.* **77**, 357 (1981).
- [15] T. Rauscher and F.-K. Thielemann, *At. Data Nucl. Data Tables* **75**, 1 (2000).
- [16] M. Arnould and S. Goriely, *Nucl. Phys.* **A777**, 157 (2006).
- [17] I. Dillmann, R. Plag, F. Käppeler, and T. Rauscher, in *Proceedings of EFNUDAT Fast Neutrons—Scientific Workshop on Neutron Measurements, Theory & Applications, Geel, Belgium, 2009* (Elsevier, Amsterdam, 2006), <http://www.kadonis.org>.
- [18] M. Weigand *et al.*, *Proc. Sci.*, NIC XII (2012) 184.
- [19] C. Guerrero *et al.* (n_TOF Collaboration), *Eur. Phys. J. Special Topics* (to be published).
- [20] H. Muthig, Ph.D. thesis, Technical University of Munich, 1984.
- [21] M. Trautmannsheimer, Ph.D. thesis, Technical University of Munich, 1992.
- [22] R. Plag, M. Heil, F. Käppeler, P. Pavlopoulos, R. Reifarh, and K. Wisshak, *Nucl. Instrum. Methods Phys. Res., Sect. A* **496**, 425 (2003).
- [23] R. L. Macklin and R. H. Gibbons, *Phys. Rev.* **159**, 1007 (1967).
- [24] U. Abbondanno *et al.* (n_TOF Collaboration), *Nucl. Instrum. Methods Phys. Res., Sect. A* **521**, 454 (2004).
- [25] R. Macklin, J. Halperin, and R. Winters, *Nucl. Instrum. Methods Phys. Res., Sect. A* **164**, 213 (1979).
- [26] S. F. Mughabghab, *Atlas of Neutron Resonances* (Elsevier, Amsterdam, 2006), 5th ed.
- [27] N. M. Larson, Oak Ridge National Laboratory Technical Report No. ORNL/TM-9179/R7, 2003.
- [28] F. Herwig, *Proc. Sci.*, NIC X (2008) 023.
- [29] T. Rauscher, *Astrophys. J. Lett.* **755**, L10 (2012).
- [30] R. D. Hoffman, S. E. Woosley, G. M. Fuller, and B. S. Meyer, *Astrophys. J.* **460**, 478 (1996).
- [31] T. Rauscher, A. Heger, R. D. Hoffman, and S. E. Woosley, *Astrophys. J.* **576**, 323 (2002).
- [32] C. Tur, A. Heger, and S. M. Austin, *Astrophys. J.* **702**, 1068 (2009).